



Electronic properties of ultrathin O-terminated ZnO (000 $\bar{1}$) on Au (111)

I. Fidelis^a, C. Stiehler^{b,1}, M. Duarte^a, C. Enderlein^c, W.S. Silva^d, E.A. Soares^e, S. Shaikhutdinov^b, H.-J. Freund^b, F. Stavale^{a,*}

^a Centro Brasileiro de Pesquisas Físicas, 22290-180 Rio de Janeiro, RJ, Brazil

^b Fritz-Haber-Institut der Max-Planck-Gesellschaft, Faradayweg 4-6, D-14195 Berlin, Germany

^c Campus de Duque de Caxias, Universidade Federal do Rio de Janeiro, Estrada de Xerém 27, 25245-390 Rio de Janeiro, RJ, Brazil

^d Brazilian Synchrotron Light Laboratory (LNLS), National Center for Research in Energy and Materials (CNPEM), Campinas, Brazil

^e Departamento de Física, ICEx, Universidade Federal de Minas Gerais, CP702, Belo Horizonte, MG, Brazil

ARTICLE INFO

Keywords:

X-ray and ultraviolet photoemission spectroscopy
Zinc oxide
Ultrathin film
Charge transfer
Polar oxides

ABSTRACT

The electronic structure of ultrathin ZnO (000 $\bar{1}$) films grown on Au (111) was investigated by scanning tunneling microscopy (STM), low-energy electron diffraction (LEED), and X-ray and ultraviolet photoemission spectroscopy (XPS and UPS). Our results show evidence of O-terminated films and formation of bulk-like ZnO (2 × 2) surface reconstruction for films with > 4 monolayers. The measurements indicate that the metal substrate plays a decisive role in the electronic structure of films since p-type doping is obtained as observed from the valence band energy shifts. Moreover, finite-size effects appear to significantly modify the Zn and O core-level energy positions. These electronic effects may account for the role of ZnO catalytic performance in ZnO/metal systems, as well as for their nanostructure optoelectronic properties.

1. Introduction

Zinc oxide crystallizes into the wurtzite structure, characterized by alternate Zn and O atomic planes, arranged in double layers separated along the *c* axis by a single Zn–O bond. The cleavage perpendicular to the *c* axis results in two polar surfaces: Zn-terminated ZnO (0001) and O-terminated ZnO (000 $\bar{1}$) [1–3]. To achieve charge neutralization, the ZnO polar surfaces undergo various crystallographic and electronic changes depending on the surface termination [2]. In general, the surface displays a charge rearrangement in order to quench the macroscopic electrostatic dipole moment through the removal of surface atoms and/or adsorption of positively (or negatively) charged ad-species [1]. These mechanisms of charge compensation are fundamental to define ZnO applications since sensor performance and catalytic behavior depend on electron transfer to the surface and ultimately to adsorbed ad-species. Several recent experimental and theoretical investigations have revealed that polarity compensation differs on each surface termination, as well as in the oxygen and hydrogen ambience [3–9]. The mechanism to achieve charge neutrality in UHV-sputter-cleaned Zn-terminated ZnO (0001) consists of either the rearrangement of the topmost layer with removal of 1/4 Zn ad-atoms and formation of a triangular morphology or, in a smaller extend, on the adsorption of

residual H[–] or OH[–] overlayers [4, 5, 10, 11]. On the other hand, charge compensation on O-terminated ZnO (000 $\bar{1}$) is characterized by its strong interaction with either water or hydrogen molecules which results on the formation of OH- surface groups, or at excellent UHV conditions, on the formation of atomic flat honeycomb Zn–O superstructures [2, 12].

The mechanisms observed on single crystal surfaces are expected to differ significantly when compared to thin ZnO films deposited on metal substrates [13]. To date, well-ordered ultrathin ZnO (0001) films have been grown on a number of well-defined metal supports (i.e., Ag (111), Au (111), Pd (111), Pt (111), and Cu (111)) [14–21]. These studies show that in films with fewer than four monolayers, the structure is depolarized by tetragonal distortion of the wurtzite structure where coplanar zinc- and oxygen-containing layers form in a graphite-like structure. This graphite-like structure is thermodynamically the most stable phase in a range of hydrogen and oxygen chemical potentials before it converts to the bulk-type wurtzite structure at larger film thickness (above ~4–5 monolayers). Interestingly, these metal-supported ultrathin ZnO (0001) films have been proposed in several studies as model systems to understand the chemistry of ZnO bulk counterparts because they can be readily investigated down to the atomic scale using conventional surface science tools. We note, however, that these films,

* Corresponding author.

E-mail address: stavale@cbpf.br (F. Stavale).

¹ Present address: Siemens AG, Rohrdamm 88, 14195 Berlin, Germany.

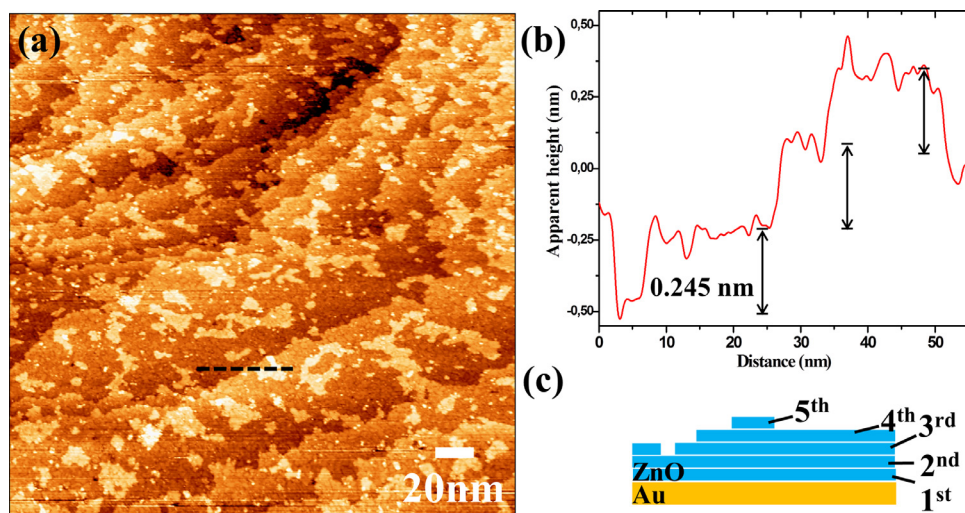


Fig. 1. Large-scale STM image of a thin ZnO film grown on Au (111) substrate at 300 K, revealing several terraces and steps (Tunneling conditions: sample bias $V_s = 2.3$ V and current $I_t = 1.0$ nA). (b) STM profile from the indicated dashed black line in (a). In the profile, the arrow indicates the STM apparent step heights. (c) Proposed ZnO layer stacking based on the features of the images.

as widely reported in the references above, exhibit distinct properties compared to their bulk counterparts. The difference lies in the competition related to the bonding preferences of Zn and O and in the electrostatic energy. Several reports in the literature on ultrathin ZnO films have shown that submonolayer films may exhibit a large superstructure (i.e., (4×4) and (6×6)) that depends on ambient conditions [19, 20]. These transformations are also related to the role of the underneath support since a larger affinity for oxygen and the varying size of the coincidence structures are decisive for the formation of various structures and ultimately responsible for the catalytic performance of ZnO/metal systems [20–22].

In a previous work, our group has reported on the preparation of ZnO films on Au (111), which is particularly convenient since it can be annealed at a sufficiently high temperature to reach thermodynamic equilibrium structures [16]. In our film preparation, ZnO grows on the (0001) direction between 1 and 30 ML in thickness, thick enough to develop the band gap of bulk ZnO. For the issue of polarity compensation at the ZnO/Au interface for films with more than four monolayers, electron transfer between the oxide and the metal underneath generates an interface dipole that aligns opposite to the structural ZnO dipole and stabilizes the wurtzite structure [23]. This leads to charge preferentially flowing from the oxide into the gold, which results in positively charged Zn^{2+} ions at the interface, while O^{2-} ions are located at the oxide-vacuum interface [24]. Indirect evidence of these O-terminated films has been discussed based on our previous STM studies [16].

In the present study, we further investigate the formation of O-terminated ZnO films on Au (111) by X-ray and ultraviolet photoemission spectroscopy (XPS and UPS), low-energy electron diffraction (LEED), and scanning tunneling microscopy (STM). The results offer additional evidence for this surface termination as well as for the formation of bulk-like (2×2) reconstruction for >4 monolayers previously not observed for thin ZnO films. Our findings are discussed in terms of the underlying mechanism for the thin film bulk-like surface reconstruction in stabilizing the polarity and the consequence for the electronic structure.

2. Experimental details

The experiments were carried out in an ultra-high vacuum (UHV) multi-chamber facility at the PGM beam line at the Brazilian Synchrotron Light Laboratory (LNLS). The UHV system is equipped with standard thin film preparation facilities and STM, XPS/UPS, and LEED. The base pressure was maintained at $\sim 5 \times 10^{-10}$ mbar and at less than 5×10^{-9} mbar during sample transfers. XPS/UPS spectra

were measured at 300 K using a SPECS PHOIBOS 150 electron analyzer using either a monochromatic Al-K α or a microwave plasma-based He-I light source. Photoemission spectra were recorded at either 15, 20° or 90° (normal emission) takeoff angle, as indicated in the figures. The binding energy was calibrated with respect to the Au $4f_{7/2}$ peak set at 84.0 eV for ZnO films grown on Au (111) and to the Zn $3p_{3/2}$ peak set at 88.5 eV for ZnO (0001) single crystals. The pass energy used for XPS survey and high-resolution spectra were 40 eV and 15 eV, respectively, and for the UPS was 5 eV. Reference spectra of clean ZnO (0001) single crystals (Mateck GmbH) were obtained by HCl 0.1 M chemical etching followed by cycles of Ar $^+$ sputtering (500 eV) and UHV annealing up to 700 K. ZnO films were prepared as described in detail in ref. [17] by the reactive evaporation of ZnO powder at 5×10^{-5} mbar of O $_2$ onto clean Au (111) single crystal with deposition rate of 0.1 nm/min determined using a quartz-micro balance. Further annealing at 800 K in 5×10^{-6} mbar O $_2$ atmosphere was performed to ensure full oxidation of the films, promoting film crystallization. The STM images were obtained in an interconnected UHV chamber equipped with a STM/AFM Aarhus-150 operated at room-temperature in the constant current mode using a chemically etched tungsten-tip.

3. Results

Fig. 1a shows an STM image of the Au (111) surface prepared by reactive deposition of ZnO at 300 K in 5×10^{-5} mbar of O $_2$ followed by annealing up to 800 K in 5×10^{-6} mbar of O $_2$. The post-annealing step promotes film crystallization which, depending on the annealing temperature and duration, leads to partial film dewetting, resulting in exposed Au herringbone clean patches. In Fig. 1a, note the formation of steps and several relatively irregular islands with heights indicated by the dashed black line profile depicted in Fig. 1b. The measured step height (~ 0.25 nm) is assigned to monoatomic steps on ZnO (0001). This value compares well with the single step height of the ZnO (0001) single crystal surface (~ 0.26 nm) and resembles the surface X-ray diffraction results found for the ZnO deposited on Ag (111) [14]. These findings concur with our previous work, in which ZnO films thicker than 4 ML grown on Au (111) display a step height of about ~ 0.26 nm [16]. Although the height measured by STM actually represents an apparent height at a particular bias voltage, we have not found significant changes as function of the applied bias. Importantly, the driving force related to the changes in the height of ZnO monolayers is connected to the polarity compensation mechanism, whereas the oppositely charged Zn^{2+} and O^{2-} alternating planes of the wurtzite structure tend to reduce their separation to minimize the associated electric dipole moment. For this reason, the constant step height

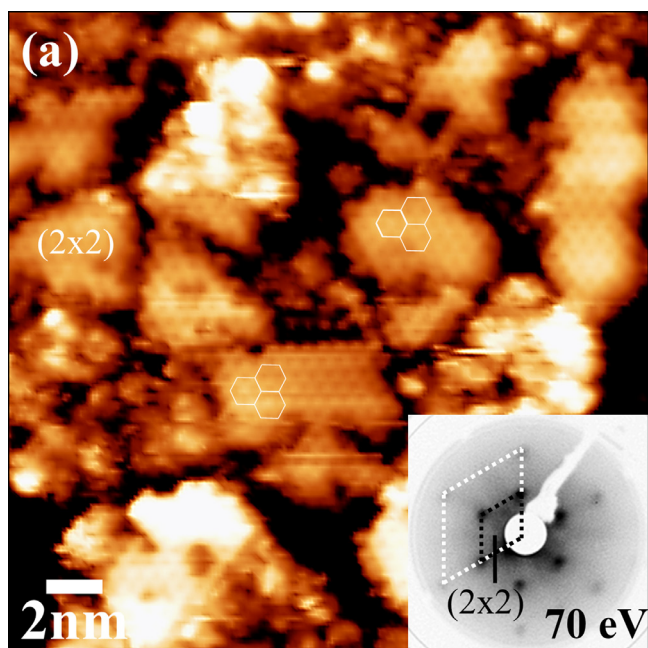


Fig. 2. STM image of an ultrathin ZnO film on Au (111) substrate at 300 K (Tunneling conditions: sample bias $V_s = 2.0$ V and current $I_t = 1.2$ nA). Inset: the corresponding LEED pattern with the primary beam energy indicated. The dashed lines indicate the ZnO film (1×1) main diffraction spots and a (2×2) surface reconstruction.

measured in our films possibly indicates that ZnO layers have been fully converted to the wurtzite structure irrespective of film thickness, and serves to assert that the film thickness is large than 4 ML. The exact film thickness is difficult to certify since the dewetting promoted by the annealing step results on a film thickness that is a fraction of the deposited film (~ 12 ML). Therefore, a tentative sketch model for the grown layers is proposed in Fig. 1c.

Additional information on the film structure comes from the high-resolution STM image shown in Fig. 2. The image reveals that the film is composed of several small flat patches delimited by ill-defined step edges. The hexagonal structure of the oxide surface (~ 0.65 nm periodicity) is readily observed in the measurements. The white hexagonal lines in Fig. 2 show that the ZnO patches are aligned along the same directions. The corresponding LEED shown in the inset displays a (1×1) hexagonal pattern with registry distance compatible with a ZnO (0001) (1×1) surface and additional spots related to a (2×2) superstructure. This superstructure can be directly assigned to the hexagonal periodicity observed on the STM images, corresponding to twice the length of the ZnO (0001) surface unit cell. In several investigations on ZnO film growth on metals, LEED patterns have displayed long-range superstructures compatible with a Moiré pattern caused by the mismatch between the ZnO (0001) lattice and the metal support [16, 18, 19, 20, 22]. In the present case, neither the long-range modulation due to the Moiré structure nor the Au (111) registry is observed in the LEED pattern. These observations support the notion that film thickness is large than four monolayers, in accordance with the sketch model proposed in Fig. 1c.

We have also investigated the electronic structure of ZnO film with XPS and UPS. Fig. 3a shows the corresponding XPS spectra for the ZnO film and, as a reference, a ZnO (0001) single crystal. The major core-level peaks for Zn, O, and Au substrates are indicated in Fig. 3a. The binding energy values found for Zn $2p_{3/2}$ and O $1s$ are 1021.5 and 530.6 eV for the ZnO film, in comparison to 1022.3 and 531.0 eV for the ZnO single crystal, respectively. Additional analysis of the peak intensities is useful to determine the O/Zn atomic ratio in the film as compared to the ZnO single crystal surface. The ZnO (0001) single

crystal has an O/Zn ratio close to the stoichiometric value of ~ 1 in contrast to the ~ 1.6 found for ZnO films. This ratio suggests that the (2×2) surface structure is likely to be related to an O-rich phase or that the ill-defined patch edges are saturated with oxygen. Fig. 3b and c show the XPS spectra at 20° and 90° takeoff angle of the O $1s$ and Zn $2p$ peaks for the ZnO film. In several studies, the presence of a substantial amount of OH groups on the ZnO surface has shown that residual hydrogen cannot be neglected even under excellent UHV conditions [25, 26]. In our study, however, we did not find evidence of OH groups by angle-resolved XPS measurements of the main O $1s$ emission peak since the typical OH component peaking at ~ 532 eV has not been observed [3]. Instead, only a single component related to oxygen bounded to Zn is seen in Fig. 3b.

More information on the electronic structure of the (2×2) phase is obtained by UPS. Fig. 4 shows the UPS spectra for the pristine ZnO film followed by UHV annealing at 850 K and 900 K compared with spectra of the clean Au (111) support and a ZnO (0001) single crystal surface. The spectra of the Au (111) support and ZnO single crystal surface serve to indicate their respective fingerprints. This way, we also compare normal emission with 15° takeoff angle in Fig. 4a and b, respectively, to identify the ZnO film Zn $3d$ and O $2p$ energy level positions with respect to the bulk ZnO. Fig. 4a shows Zn $3d$ and O $2p$ peaks located at 10.8 and 4.5 eV, respectively, for the ZnO (0001) single crystal surface. These values compare well with the binding energy observed in previous reports for either the Zn-terminated ZnO (0001) or O-terminated ZnO (0001) single crystals surfaces [3, 27]. The figure also shows the UPS spectra for the Au (111) support, characterized by the Au d -band structure and its surface state (SS) at ~ 0.5 eV. The comparison with the film spectra allows labeling the three peaks related to Zn $3d$ (p_1) and O $2p$ (p_2 and p_3) for the ZnO film. Although the overall spectral features are strongly overlapped by the Au d -band structure, UHV annealing promotes film dewetting, as one compares peak p_1 before and after annealing, thus highlighting the ZnO film contribution to the spectra. The persistence of the gold surface state (SS) contribution indicates that open patches may be present after the final annealing step. In Fig. 4b, the spectra taken at 15° takeoff angle are convenient to identify spectral features related to O $2p$ (indicated by p_2 and p_3 labels). Herein, we take advantage of the fact that the ZnO valence band features are not expected to disperse strongly under measurement conditions and that the Au $3d$ structure is clearly suppressed from 4.5 to 2 eV. Thus, after UHV annealing, we firstly note that the labeled p_2 contribution decreases as the film is detached from the surface and, secondly, that the labeled p_3 contribution persists. These features are hardly observable in Fig. 4a, except from the small shoulder indicated by p_3 . Therefore, the valence band of ZnO film is assigned to Zn $3d$ (p_1), O $2p$ -Zn $4sp$ hybridized band (p_2), and O $2p$ (p_3) at 10.1, 4.4, and 3.4 eV, respectively.

4. Discussion

In our previous investigation into ZnO films grown on Au (111), we proposed that the stacking sequence on electronegative gold start with Zn atoms at the oxide-metal interface, leading to an O-terminated film where $1/2$ ML H^+ ion adsorbates are involved in electric dipole moment cancellation [16]. In the present study, the emergence of a (2×2) superstructure and the valence band emission features support the notion of an O-terminated film and indicate that the dipole compensation for the >4 ML films can also be similar to that found for ZnO (0001) single crystal surface. For O-terminated ZnO single crystals, Lauritsen et al. have reported that the surface may be converted to a flat (2×2) honeycomb or (5×5) structures depending on the hydrogen/oxygen chemical potentials [12, 28]. The authors have proposed that the most stable hydrogen-free structure is a stoichiometric (2×2) surface, consistent with the XPS spectra of our single component O $1s$. Moreover, our STM images display periodicities compatible with (2×2) honeycomb structures, with an average corrugation of ~ 0.25 nm between the protrusions and troughs, which compares quite

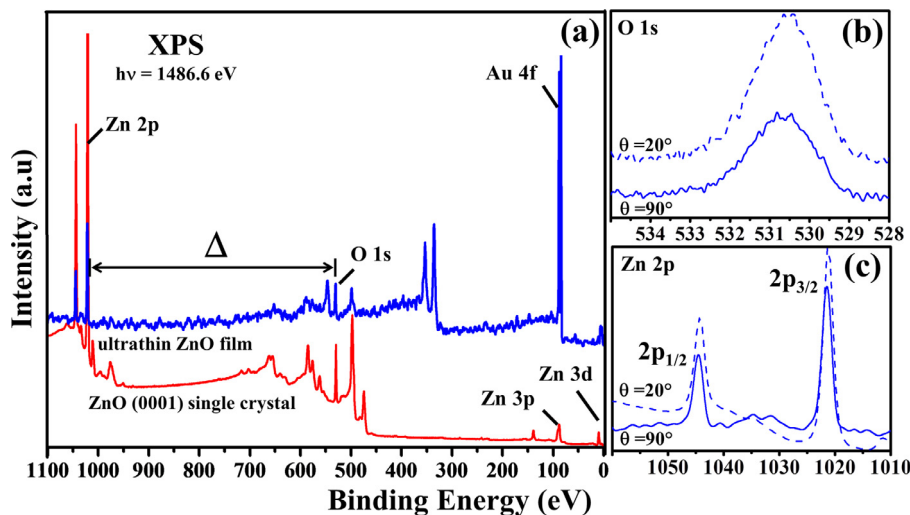


Fig. 3. (a) XPS spectra of ultrathin ZnO film on Au (111) substrate (blue curve) and of a ZnO (0001) single crystal surface at 300 K. (b) O 1s and (c) Zn 2p core-level spectra of ultrathin ZnO film measured at the takeoff angles indicated. The spectra are offset and the overall intensity adjusted for clarity.

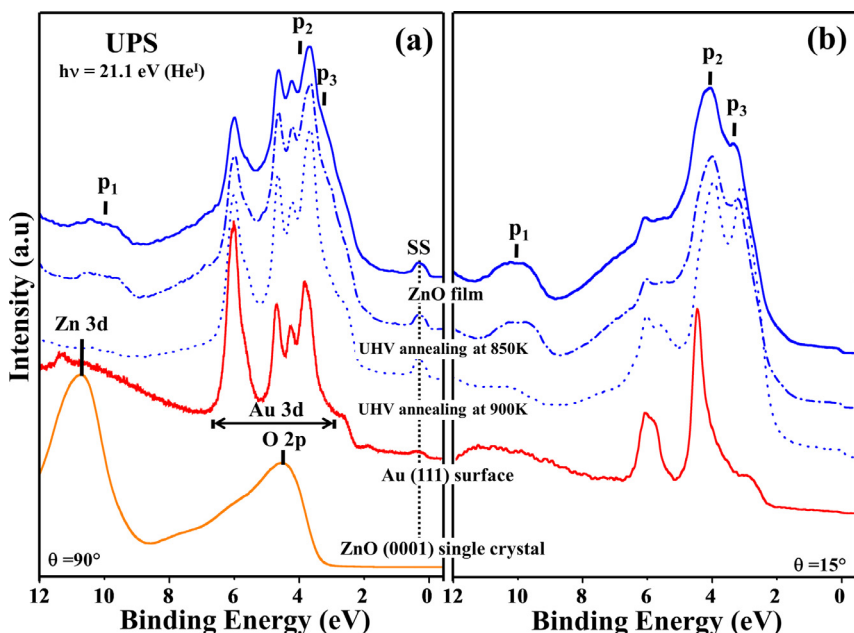


Fig. 4. (a) UPS spectra at normal emission (90°) and (b) at 15° takeoff angle of pristine ZnO film, after UHV annealing at 850 K and UHV annealing at 900 K, as indicated. Two reference spectra are indicated in the figure ZnO (0001) single crystal surface and a clean Au (111) substrate. The spectra were acquired at the takeoff angles indicated, are offset and the overall intensity adjusted for clarity.

well to a previous observation on a similar (5×5) honeycomb structure [12, 28].

The O termination has important consequences for the electronic structure of the film. The further analysis of the valence band region reveals band shifting upward with respect to the Fermi level. One can clearly recognize the Zn 3d shift toward lower binding energies of about 0.7–0.8 eV considering the bulk 3d energy level position. Apparently, the intrinsic dipole of the ZnO film leads to a potential difference across the film. This means that even for the (2×2) surface structure either a charge transfer occurs from the ZnO film to the Au support, decreasing the apparent overall binding energy, or even, alternatively, the film with (2×2) surface structure exhibits a smaller band gap compared to the bulk ZnO. The overall behavior of the valence band can be understood as an interplay between surface charge and image charge effects. The electric dipole developed as the ZnO film grows is screened by the metal substrate. We argue that an image charge of opposite sign forms in the gold substrate, which results in the creation of an interface dipole. The interface dipole between the gold substrate and the ZnO film shifts the bands up with respect to the Fermi level. Therefore, on one

hand, the O-terminated surface may achieve charge neutralization reconstructing itself. On the other hand, electrons may be transferred from the Zn-terminated side to the gold substrate, as with the mechanism observed for hydrogen adsorbed on thicker ZnO films [16]. As a result, a sort of p-type doping is obtained, as the top of the film's valence band shifts toward the metal substrate's Fermi level, which contrasts with commercial bulk ZnO single crystal surfaces that generally display n-type characteristics [2]. This shift towards the Fermi level further supports our interpretation of a hydrogen-free O-terminated surface since the Zn-terminated surface would result in downward band bending and the hydrogen-decorated surface would exhibit no shift because of electrical dipole quenching. These findings are consistent with those of Bieniek et al. for the DFT calculations of ultrathin ZnO films, where O-terminated ZnO multilayers emerge as the dominant surface termination once ZnO films reach a thickness larger than four layers in several noble metal substrates [22].

Additional consequences for the electronic structure of thin ZnO film appear due to its limited thickness. When analyzing the energy level positions in Fig. 3a, we note a contraction of the core-level energy

distance (Δ) comparing the Zn 2*p* and O 1*s* for the ZnO film (Δ_{film}) with the ZnO bulk single crystal (Δ_{bulk}). The difference between the film and bulk ($\Delta_{\text{film}} - \epsilon\Delta_{\text{bulk}}$) is given by $\sim 0.3\text{--}0.4$ eV, as indicated in Fig. 3a. Although it is relatively difficult to unequivocally assure the energy level positions in the valence band region due to Au *d*-band overlapping, similar energy level contraction appears also when we compare the relative energy difference of the Zn 3*d* and O 2*p* bands of the film to the bulk single crystal. The energy level contraction and binding energy shift reflect the resultant changes to either the initial or final-state configurations of the photoemission processes possibly associated with the charge transfer or lattice parameter changes in the ZnO film [29–31]. To address these issues, we point out the confinement effect on ZnO nanostructures recently reported by Sponza et al. [13]. In their work, the authors used DFT calculations to investigate changes in the energy level positions related to electrostatic forces in several ZnO polymorphs. The low dimensionality of the ZnO films imposes variations in the energy level position related to the Madelung potential across the finite oxide structure. Importantly, the authors reported that in ZnO films with few monolayers, the Madelung potential is reduced and, therefore, the effective energy levels of oxygen and zinc are closer to each other than in the bulk, resulting in bonds that are likely to be more covalent [13].

5. Conclusions

We investigated the electronic structure of O-terminated ZnO (000 $\bar{1}$) films with > 4 monolayers on Au (111) using XPS and UPS. We observed notable changes in the electronic properties of the thin film compared to its bulk counterpart. These changes are apparently related to two major effects: charge transfer from the substrate, related to the Fermi level of the substrate, and possible reduction of the Madelung potential, due to finite-size effects. Firstly, our results show that the polar surface is O-terminated and displays a (2 × 2) reconstruction similar to that found for O-terminated ZnO (000 $\bar{1}$) single crystals. It is intriguing, however, that charge transfer occurs from the surface to the substrate even after surface reconstruction, whereas a sort of p-type doping is obtained. Secondly, although widely discussed for several oxide surfaces, core-level shifts and energy level contraction are generally underreported for ultrathin ZnO films. Nevertheless, our results indicate that new electronic properties may be induced on ZnO films grown on metal substrates which may serve as a pathway to effective p-type doping for optoelectronic devices. For this reason, further angle-resolved photoemission spectroscopy (ARPES) experiments, as well as, transport measurements are mandatory to further elucidate the mechanism related to the doping characteristics on ZnO/metal systems.

Acknowledgments

We gratefully acknowledge the assistance of the LNLS staff during beam time. This work was supported by the CNPq, FAPERJ, Alexander

von Humboldt Foundation, and the Max-Planck Partnergroup Program grants. F.S thanks Prof. Emilia Annese for her critical reading. C.S thanks for the fellowship grant from the Studienstiftung des deutschen Volkes. E. A. S thanks FAPEMIG and CNPq for financial support. C. E wishes to thank ICAM for financial support.

Supplementary materials

Supplementary material associated with this article can be found, in the online version, at doi:10.1016/j.susc.2018.10.007.

References

- [1] C. Noguera, *J. Phys. Condens. Matter* 12 (2000) R367.
- [2] C. Wöll, *Prog. Surf. Sci.* 82 (2007) 55.
- [3] R. Heinhold, G.T. Williams, S.P. Cooil, D.A. Evans, M.W. Allen, *Phys. Rev. B* 88 (2013) 235315.
- [4] G. Kresse, O. Dulub, U. Diebold, *Phys. Rev. B* 68 (2003) 245409.
- [5] O. Dulub, U. Diebold, G. Kresse, *Phys. Rev. Lett* 90 (2003) 016102.
- [6] J. Lahiri, S. Senanayake, M. Batzill, *Phys. Rev. B* 78 (2008) 155414.
- [7] R. Lindsay, C.A. Muryn, E. Michelangeli, G. Thornton, *Surf. Sci.* 565 (2004) 283.
- [8] M. Valtiner, M. Todorova, G. Grundmeier, J. Neugebauer, *Phys. Rev. Lett.* 103 (2009) 065502.
- [9] L.F.J. Piper, A.R.H. Preston, A. Fedorov, S.W. Cho, A. DeMasi, K.E. Smith, *Phys. Rev. B* 81 (2010) 233305.
- [10] Th. Becker, St. Hövel, M. Kunat, Ch. Boas, U. Burghaus, Ch. Wöll, *Surf. Sci.* 486 (2001) L502.
- [11] M. Valtiner, M. Todorova, J. Neugebauer, *Phys. Rev. B* 82 (2010) 165418.
- [12] J.V. Lauritsen, S. Porsgaard, M.K. Rasmussen, M.C.R. Jensen, R. Bechstein, K. Meinander, B.S. Clausen, S. Helveg, R. Wahl, G. Kresse, F. Besenbacher, *ACS Nano* 5 (2011) 5987.
- [13] L. Sponza, J. Goniakowski, C. Noguera, *Phys. Rev. B* 93 (2016) 195435.
- [14] A. Shiotari, B.-H. Liu, S. Jaekel, L. Grill, S. Shaikhutdinov, H.-J. Freund, M. Wolf, T. Kumagai, *J. Phys. Chem. C* 118 (47) (2014) 27428.
- [15] C. Tusche, H.L. Meyerheim, J. Kirschner, *Phys. Rev. Lett.* 99 (2007) 026102.
- [16] F. Stavale, L. Pascua, N. Nilius, H.-J. Freund, *J. Phys. Chem. C* 118 (25) (2014) 13696.
- [17] F. Stavale, L. Pascua, N. Nilius, H.-J. Freund, *J. Phys. Chem. C* 117 (2013) 10552.
- [18] X. Deng, K. Yao, K. Sun, W.-X. Li, J. Lee, C. Matrangola, *J. Phys. Chem. C* 117 (2013) 11211.
- [19] G. Weirum, G. Barcaro, A. Fortunelli, F. Weber, R. Schennach, S. Surnev, F.P. Netzer, *J. Phys. Chem. C* 114 (2010) 15432.
- [20] B.-H. Liu, M.E. McBriarty, M.J. Bedzyk, S. Shaikhutdinov, H.-J. Freund, *J. Phys. Chem. C* 118 (2014) 28725.
- [21] B.-H. Liu, I. Groot, Q. Pan, S.K. Shaikhutdinov, H.-J. Freund, *Appl. Catal. A* 548 (2017) 16.
- [22] B. Bieniek, PhD thesis, Technical University of Berlin, TU Berlin, 2016.
- [23] S. Benedetti, P. Torelli, S. Valeri, H.M. Benia, N. Nilius, G. Renaud, *Phys. Rev. B* 78 (2008) 195411.
- [24] Y. Pan, S. Benedetti, S. Valeri, C. Noguera, L. Giordano, J. Goniakowski, N. Nilius, *J. Phys. Chem. C* 116 (2012) 11126.
- [25] B.-H. Liu, J.A. Boscoboinik, Y. Cui, S. Shaikhutdinov, H.-J. Freund, *J. Phys. Chem. C* 119 (2015) 7842.
- [26] X. Deng, D.C. Sorescu, J. Lee, *J. Phys. Chem. C* 120 (2016) 8157.
- [27] K. Ozawa, K. Mase, *Phys. Rev. B* 83 (2011) 125406.
- [28] R. Wahl, J.V. Lauritsen, F. Besenbacher, G. Kresse, *Phys. Rev. B* 87 (2013) 085313.
- [29] P.S. Bagus, A. Wieckowski, H.-J. Freund, *Comput. Theor. Chem.* 987 (2012) 22.
- [30] P.H. Citrin, G.K. Wertheim, *Phys. Rev. B* 27 (1983) 3176.
- [31] J.N. Andersen, D. Hennig, E. Lundgren, M. Methfessel, R. Nyholm, M. Scheffler, *Phys. Rev. B* 50 (1994) 17525.